LA-UR-17-22660

Approved for public release; distribution is unlimited.

Title:	Verification and Validation of Unstructured Mesh Tracking in the MCNP® Code Version 6.2
Author(s):	Roger L. Martz and Joel A. Kulesza
Intended For:	General Reference / MCNP® Website
Issued:	April 2017

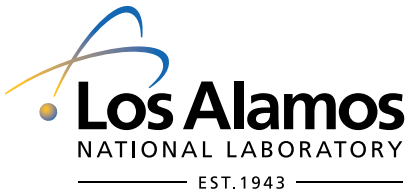

This page intentionally left blank.

Verification and Validation of Unstructured Mesh Tracking in the MCNP® Code Version 6.2

Roger L. Martz and Joel A. Kulesza
Monte Carlo Methods, Codes, and Applications
X-Computational Physics Division
Los Alamos National Laboratory

April 2017

1 Introduction

This report documents the recent changes to a top level tracking routine from the Revised Extended Grid Library (REGL) for the unstructured mesh (UM) feature in MCNP6 [1]. This tracking routine is the one used to track within an UM pseudo-cell, what was once referred to as a part. Verification and validation (V&V) work is presented using various benchmark problems where the geometry is represented with an UM. It is assumed that the reader is familiar with the general features of the UM, its terminology, and its implementation in MCNP6.

2 Tracking Methodology

One of the main components of Monte Carlo transport codes is ray-tracing particle paths through the problem geometry from birth to termination. Source routines in a code like MCNP6 generally provide particle starting position, energy, direction, and cell number. With this information in hand, the code looks for the exit location on the cell's enclosing surface. If this distance to surface is less than any other distance to event, such as distance to collision, the particle is advanced to this exit location with the appropriate adjustment of parameters including a determination of the new cell it will enter. Then, the process is repeated using the properties associated with the new cell. For the purposes of this report, this process is referred to as immediate mode tracking (IMT) because the process is only concerned with the immediate locale the particle encounters. Historically, this has proven to be efficient (in a method that is known to be inefficient because of its statistical nature and numerous conditional selections) in that no time is spent in speculative tracking.

While there are a number of aspects to particle tracking on MCNP6's UM that are worth discussing, the remainder of this section is devoted to the part of the REGL that involves tracking within a pseudo-cell. In fact, the discussion will be limited to the high-level aspects

only because this is what was refactored for the 6.2 version. There were two primary reasons for the refactor: 1) make the coding less convoluted, and 2) make the code faster, if possible. Item 1) is important so that future code developers will have an easier time understanding how the code works. Item 2) is expected to be highly problem dependent; evidence of this can be seen in the results sections below.

2.1 Approach Before Version 6.2

From its inception through the current version of MCNP6, the UM tracking algorithm in the REGL has followed the IMT paradigm with the added complication that tracking takes place through the elements that subdivide the cell so that path lengths may be obtained for each element through which the particle passes. Obviously, this requires more intersection calculations than what are required when tracking on the traditional constructive solid geometry (CSG).

When the intersection occurs on an element's face where the nearest neighbor on the other side of that face is definitely known, transition to the next element along the particle's path is easy. However, there are several conditions under which this is not the case:

1. The current element's face is on the pseudo-cell's surface and will either exit into another pseudo-cell or the background region. Hence, the nearest neighbor number is 0.

2. The particle is exiting through a vertex or edge into an element that is not a nearest neighbor. (For example, a tetrahedron has 4 faces and hence 4 nearest neighbors, but many tets many share a vertex or an edge without being one of the 4 nearest neighbors.)

3. A particle stalls at a vertex or an edge because the trajectory is such that the distance to intersection is small (~10^{-9} cm) and the algorithm oscillates between 2 or more elements.

Condition #1 above was a known issue from the beginning of the REGL development. Handling of conditions #2 and #3 above has evolved from what at first sight may be an incoherent treatment of a number of special cases to fit the IMT paradigm to a simplified treatment with a look-ahead approach to construct the particle's path. Up until MCNP Version 6.2 when the look-ahead paradigm was introduced to handle conditions #2 and #3 above, all previous versions of the code relied on special cases to handle the aforementioned conditions.

Details of how the earlier versions of MCNP6 handled the special cases will not be discussed in detail in this report. Some components of the special case handling evolved into the look-ahead approach that is described below. One of the factors affecting the evolution of the UM tracking was the handling of the nearest neighbors. Up through Version 6.1 of the code, the nearest neighbor lists were built on the fly if they did not exist. After the neighboring element was found, a containment check was performed to verify that the intersection point was on its surface. Then an intersection check was done to determine if the particle had an intersection with that element. For Version 6.1.1, most of this was abandoned except for the use of the nearest neighbor lists which were now created during input processing (that could be handled in a parallel manner via MPI, when requested [2]). Version 6.1.2 was LANL's in-house development version for awhile after the release of 6.1.1 to the code center at RSICC. Starting in Version 6.1.2 testing of unique UM facet numbers was implemented as a means of reducing the checking needed for the special cases.

Part of the special case checking in these early REGL versions revolved around the information that was obtained by finding all intersection points with elements constituting a part. This is what evolved into the foundation for the look-ahead method discussed below.

2.2 Look-Ahead Tracking

The look-ahead tracking (LAT) method is one that is used whenever certain conditions, discussed in the previous sections, arise while tracking within a pseudo-cell. This method deviates from the previously discussed IMT paradigm by approaching the tracking problem from a different perspective. The central tenets of LAT are two questions: 1) If the particle continues on a straight path, what is the path length in each element of this pseudo-cell? 2) With the path length by element information, how can the particle's path be reconstructed starting with its current location? The reader should recognize that LAT differs from the IMT paradigm in that there are, more than likely, speculative calculations done that are discarded. Also, the reader should recognize that the LAT approach may be worth exploring as a potential speedup of UM calculations with GPUs.

LAT tenant #1 was actually used routinely in part in code versions prior to 6.2 whenever the REGL couldn't determine the next element along the path. Using it can be quite costly, particularly if a pseudo-cell has a large element count and it is needed more than once in the tracking loop. If at any time the distance the particle is required to travel is much less than the total path length found through all elements, much of the calculations are for naught. As will be discussed below, the LAT is invoked only once in the refactored high-level tracking loop used for tracking within pseudo-cells.

LAT tenant #2 is inherently serial in nature as the method must reconstruct the particle's path starting from its current location. The starting point for the implementation of this tenant is an ordered list of intersection points. As the particle's path is constructed using this ordered list and the elemental path lengths, the algorithm must check that the requested travel distance is not exceeded. If the requested travel distance is exceeded, appropriate calculations must be made to find the stopping point and the element containing it. A crucial part of implementing this tenant is discarding elements (and their path lengths) that contribute to one of the previously described stall conditions when multiple elements are involved. Usually these paths lengths are very small and can be viewed as redundant. Whichever element and its associated path length is chosen is probably good enough to use in the stall region. One way to view this is that all of these very small path lengths are consolidated and assigned to one element. At no point in the path construction process is a path produced with gaps.

2.3 Top-Level Tracking Routine

The following is an outline of the top-level tracking routine (found in subroutine `regl_track_um`) used when tracking within a pseudo-cell.

- IMT: Find the intersection point in the current element. If the face containing the intersection point has a nearest neighbor, continue looping via IMT after the appropriate accounting information has been recorded and termination checks performed.
- LAT: If the distance to intersection is very small and no nearest neighbor has been found or the nearest neighbor element is the same as the previous element, track through the rest of the pseudo-cell using LAT.
- If the particle is not stopped in the current pseudo-cell, call the routine to check hitting other pseudo-cells. If another pseudo-cell is not hit, it is assumed that the particle is transitioning to the background region. In either case, set the appropriate return variables and exit to the calling routine.

A main assumption when this routine is called is that the particle will be at some location within a known element seeking to escape that element to a neighboring element as it tracks through the pseudo-cell. This is not always the case. Sometimes the particle is on an edge (or vertex) headed out of the element or possibly the pseudo-cell. In this case the IMT as implemented in REGL fails immediately and the rest of the routines (LAT, etc.) must be able to correctly compensate.

2.4 Summary of REGL Tracking Integration

MCNP6 handles both unstructured and structured meshes in an hybrid geometry approach where the meshes must be contained in a mesh universe with a background region. Traditional CSG can be specified to any degree outside of the mesh universe, but not inside of it. Multiple mesh universes are permitted. There are no restrictions on how particles track into or out of these universes.

In MCNP6, all calls to REGL for UM tracking are handled through the Revised Grid Library Interface (RGLI) routines in order to maintain modularity with the library. If the particle is at a source or collision site inside the UM, the appropriate RGLI routine is called to invoke the REGL tracking routine discussed in this report. If the particle is outside of the mesh in the universe background region, the appropriate RGLI routine is called that will in turn invoke the REGL routine to determine where the particle will enter the mesh. If the particle doesn't hit the mesh, normal CSG tracking is invoked.

3 Test Systems

Two different Linux computer systems and one Apple workstation were used in to run test problems for this report. They are described next.

3.1 System 1 — Blowpop

This system is a workstation with 2 quad-core Intel Xeon model E5540 chips running at 2.53 GHz. Each CPU core has 256 KB of L1 cache, 1 MB of L2 cache, and 8 MB of L3 cache (DDR3 @ 1066 MHz). All CPUs share 74 GB of RAM. The operating system is RedHat 6.

3.2 System 2 — Snow

This system is a cluster and has over 368 nodes where each node has two 18-core Intel Xeon Broadwell [ES-2695v4] sockets for a total of 36 CPUs per node. The CPUs run at 2.1 GHz. Each node has 128 GB of DDR4 RAM (2400 MHz). The 45 MB of SmartCache is shared among the 18 cores of a socket. This system uses the Clustered High Availability Operating System (CHAOS), a modified version of RedHat Linux

3.3 System 3— Steele

This system is a Mac Pro running OS X 10.11.6 (El Capitan). It has a 2.7 GHz 12 Core Intel Xeon E5 chip with 64 GB of RAM (1866 MHz DDR3 ECC), an L2 cache of 256 KB, and an L3 cache of 30 MB.

4 Test Problems

This section provides a brief overview of the three criticality benchmarks and the two fixed-source benchmarks used in this work.

4.1 HEU-MET-FAST-007 : Case 37

The HEU-MET-FAST-007 series of criticality benchmark problems taken from Reference 3 consists of forty-three critical experiments, involving moderated slabs of highly enriched uranium metal (93.15 wt. % ^{235}U), conducted at the Oak Ridge National Laboratory (ORNL) in 1967. The unreflected experiments consisted of uranium metal slabs interleaved with polyethylene, plexiglass, or teflon. Some of the experiments moderated by polyethylene also had a six-inch polyethylene reflector.

Not all configurations were fast systems; it is for that reason that Case 37 from this series was selected. From Table G.1 of Volume II of Reference 3 that describes the spectra of neutrons causing fission, it can be seen that 22.71% were from the thermal range, 34.88% were from the intermediate range, and 42.41% were from the fast range. The Case 37 configuration has polyethylene slabs interleaved with the uranium slabs and the polyethylene reflector around the slabs.

For this work the original MCNP5 input deck from Reference 3 with its ENDF/B-VI cross section specifications was re-run in MCNP6 as a control case. The original lattice CSG input was converted to a non-lattice CSG input description. The specifications from the input decks were then used to construct an UM model in Abaqus / CAE. The plate assembly was constructed from 3 parts: full fuel plate, half fuel plate, full moderator plate. The reflector was constructed from 6 parts. Each part was meshed separately with first order hexahedra. Each plate was constructed with 200 elements. The element count for the entire assembly totaled 3586 hexahedra. Certainly, the number of elements for this geometry could have been reduced and the volume / masses of components maintained. However, no attempt was made to reduce the element count to improve the run times.

4.2 IEU-MET-FAST-007 : Two-Zone Homogenized Model

This problem is an adaptation of the Big Ten critical benchmark [3]. Big Ten was a large, mixed-uranium-metal, cylindrical core with 10% average ^{235}U enrichment surrounded by a thick ^{238}U reflector. The name "Big Ten" reflects both its total mass of uranium (10 metric tons) and the average ^{235}U enrichment of its core (10%).

A simplified two-zone homogenized model similar to the model of Big Ten used by the Cross Sections Evaluation Working Group (CSEWG) was developed on the detailed model (see Volume III, Section D.2 of Reference 3 where the assumptions for this model are detailed). For the current work, ENDF/B-VII cross sections were used. The models in this work were taken from Reference 4.

4.3 HEU-MET-FAST-001 : Simple Bare Sphere

The models for this work were taken from the Reference 5 work where the Godiva critical benchmark was used [3, 6] and do not use the simple one sphere description that is often used for this benchmark. With the MCNP6 CSG capability, it is possible to model polyhedrons bounded

by planes with an arbitrary orientation. Because finite elements of the first-order tetrahedral type are guaranteed to have planar faces, it is possible to reproduce these finite elements in MCNP6 with cells defined by arbitrary planes [1]. From the same Abaqus input file used in the MCNP6 calculations with the UM, it is possible to create an equivalent representation of the first-order tetrahedra using arbitrary polyhedral cells (APCs) with the CSG capability. To make it convenient to describe what is known as "the outside world" in MCNP6 (i.e., the phase-space outside of the geometry of interest), each benchmark geometry was placed in a box of air so that one macrobody surface represented the boundary between the geometry of interest and the outside world. All of the geometry inside this macrobody was described with either a mesh of finite elements or with APCs. These boxes were not tightly fit around the spheres because space was needed to generate well-formed elements adjacent to the outer spherical surfaces. In the course of this work, like the Reference 5 work, the number of finite elements and APCs was varied to look at code performance as a function of elements and cells as well as results. This permits a consistent assessment when different physics options are specified.

In the Reference 5 work, the material and source descriptions were altered so that three unique problems used the same geometries. The only set from that work used in this work is the well-known Godiva critical bare-sphere benchmark [3, 6]. Lady Godiva, as the setup was called, is an example of a fast neutron critical system. It was a simple geometry, consisting of a 52.42 kg sphere of U (93.71) — 93.71% U-235 enriched. The density of the system was measured at 18.74 g/cm^3. These data correspond to a sphere of radius equal to 8.741 cm.

4.4 Kobayashi Analytical Benchmark

The Kobayashi benchmark suite [7] was created primarily to evaluate the accuracy of three-dimensional deterministic radiation transport codes using one-group fixed-source problems capable of being solved analytically. As such, it consists of three geometric configurations characterized by a uniform volumetric isotropic source within a void region within a shield region where the source and shield are composed of a purely absorbing material or a material that it 50% absorbing and 50% scattering. The benchmark flux solutions in the pure absorber cases were calculated directly using numeric integration whereas the 50/50 flux solutions were obtained using long-running Monte Carlo calculations performed with the GMVP code [7, 8].

In Reference 7, each of the benchmark problems is defined using reflective boundaries along the cardinal planes thus representing one-eighth of a physical volume surrounded by a vacuum boundary. MCNP6 cannot use reflecting boundaries with point detectors. Hence, all MCNP6 geometries are defined for all eight octants and surrounded by a vacuum.

To date there have been primarily two methods (work flow paths) used to generate UM input for MCNP6: Abaqus/CAE [9] and Attila4MC [10]. Both conclude by generating an Abaqus mesh input file [2] for use by MCNP6. More details for generating UM input for MCNP6 can be found in References 2 and 11. Additional details on the UM Kobayashi models can be found in Reference 12.

Previous work [13] analyzed the Kobayashi benchmarks with MCNP5 using MCNP's traditional CSG system and multi-group (MG) cross sections. This current work, and the work of Reference 12, also used the MG cross sections with the UM models. In addition, semi-analytic continuous-energy (CE) cross sections were generated and used here for this work and that of Reference 12.

The problem used in this verification work is problem #1 from the Kobayashi benchmark suite [7] as described in Reference 12. Specifically, it is best described as a series of nested cubes

with the central cube, 20 cm on a side, acting as an isotropic volume source composed of the same material as the shield (either pure absorber or 50/50 absorber/scatter). Surrounding the source is a cubic void with an outer side length of 100 cm. Surrounding the void is a cubic shield with an outer side length of 200 cm. Dimensioned plan, elevation, and 3-D perspective views of the geometry are available in Reference 7. A cutaway isometric view of the tetrahedral and hexahedral UM generated with Abaqus is shown in Figure 1. The first-order tetrahedral UM generated with Attila4MC is shown in Figure 2 for two arbitrary levels of mesh refinement: coarse and fine. Total UM node and element counts for UM models are given in Table 1.

As stated in Reference 12 for the Kobayashi UM models, the UM geometry is defined consistent with the benchmark "reality" with no arbitrary geometry introduced for the purpose of applying cell-based variance-reduction techniques, which is a departure from the approach taken in the original CSG executions [13].

Figure 1: Tetrahedral (left) and Hexahedral (right) Abaqus-generated UM

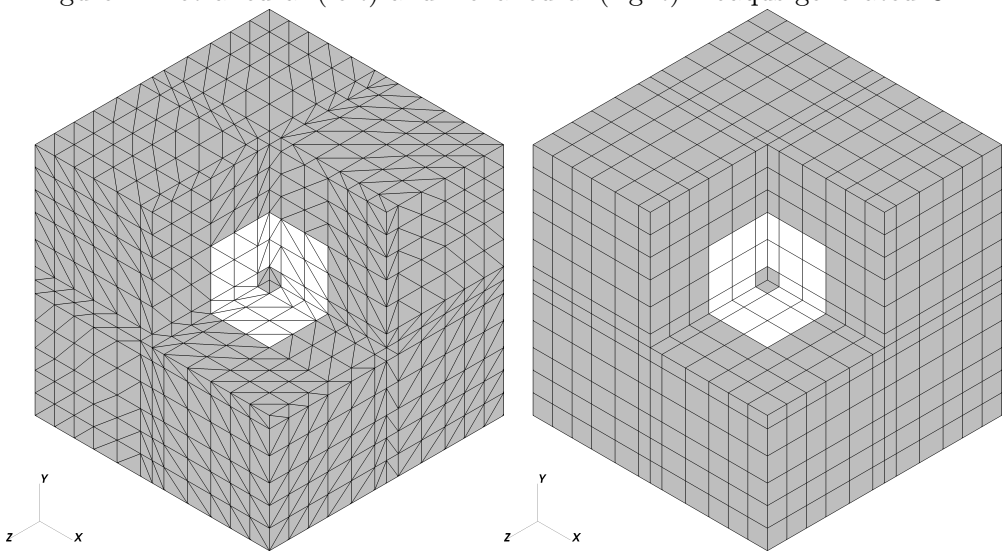

Table 1: Kobayashi Unstructured Mesh Node and Element Counts

Mesher	Element Type	Nodes	Elements
Abaqus	First-order Tetrahedrons	3422	17430
Abaqus	First-order Hexahedrons	2197	1728
Attila4MC	First-order Tetrahedrons (coarse)	89	228
Attila4MC	First-order Tetrahedrons (fine)	16442	60633

4.5 Ueki Neutron Shielding Benchmark

The Ueki benchmark suite is a series of experiments characterized by a small spontaneous fission source of ^{252}Cf centered within a paraffin cube with a conical cutout facing a detector, with one or several shields of thickness T and various shielding materials between the source and detector as shown in Figure 3. Of the configurations provided in the experimental description [14], we most recently [15] focused on those configurations with a single graphite shield of either

Figure 2: Coarse (left) and Fine (right) Attila4MC-generated UM

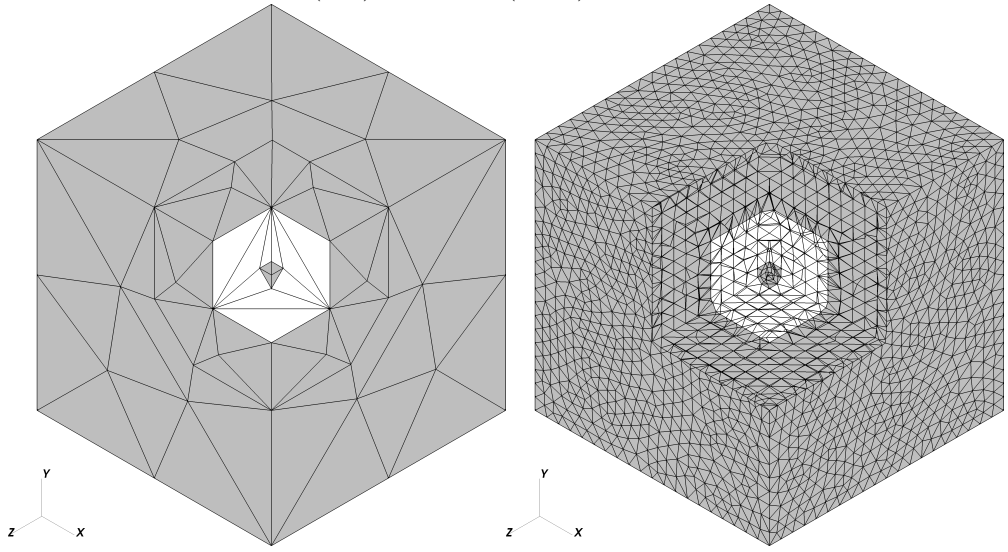

thickness $T = 2$, 5, 10, 15, 20, 25, 30, or 35 cm. This benchmark was most previously analyzed in Reference 16 where it was noted that tabulated results were not provided for the cases with the graphite shield. As such, the lin-log plot provided in Reference 16, Figure 7-2, was digitized [17] to extract the experimental dose attenuation factors for graphite. When this digitization was performed, a conservative 5% uncertainty was assigned to account for experimental and digitization errors.

After publication of [15] we were able to locate a copy of Reference 14. This reference contained the neutron dose equivalent rates when the KRAFTON N2 shield material was used. KRAFTON N2 is a soft ceramic produced by solidifying a high-hydrogen alloy and hydroxides, such as titanium-, aluminum-, and lithium-hydroxides in addition to boron and gadolinium oxides, for a total of 16 elements [14], in an attempt to attenuate both fast and thermal neutrons. The KRAFTON N2 material was used in this work with the shield thicknesses listed above. ENDF/B-VII cross sections where used for all nuclides.

The experiments were modeled using both CSG and UM with a small cubic F4 (track-length) tally and with an F5 (point detector) tally centered within the cube as surrogates for the radiation detector. Weight windows were generated with ADVANTG [18] for each of the KRAFTON models and used along with the default variance reduction techniques (i.e., weight cutoff and implicit capture for the random transport and the default point detector roulette game) for both the KRAFTON and graphite calculations. Both the CSG and the UM models use materials for paraffin, KRAFTON N2, and air based on the compositions and densities provided in References 14, 19. For both geometries, the source is positioned at $x = 0.5$ cm in order to prevent it from being coincident with CSG cell or UM pseudo-cell boundaries. The source is specified with an energy distribution following the MCNP6 Watt fission spectrum (function 3) using MCNP6 distribution parameters $a = 1.025$ and $b = 2.926$. When specifying the two tallies, the dose response function from Reference 20 is used, and the results are normalized to Sv $\cdot$ h^{-1} $\cdot$ source-particle^{-1}. This permits a direct comparison to the experimental results of Reference 14.

Several UM models of this experiment were created for the Reference 15 work. The At-

Figure 3: Ueki benchmark geometry (dimensions are in units of centimeters).

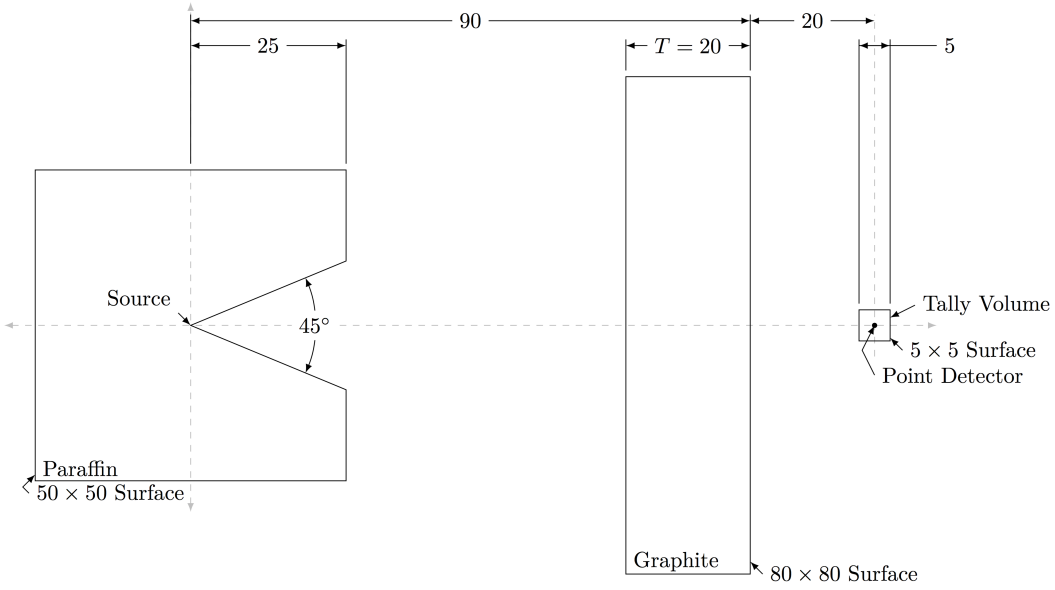

tila4MC 1st order tet models and the Abaqus 1st order hex models were used in this current work. More details on the UM models can be found in Reference 15.

5 Verification and Validation

This section discusses the results of calculations from the test problems outlined in Section 4.

5.1 HEU-MET-FAST-007 – Case 37

Calculations for this problem considered three different geometry descriptions, described in Section 4.1, and three different tracking paradigms. The lattice and non-lattice CSG descriptions used the traditional MCNP6 tracking while the UM description was studied with both the 6.1.2 and 6.2 versions of the code. This culminated in results for four situations. For each situation, ten independent runs were performed and the answers averaged and a sample standard deviation was calculated.

Reference 3 stated that the experimental k_{eff} for the Case 37 arrangement was 0.9988 (Reference 3 Table 2) and their calculated value with MCNP5 was 1.0053±0.0002 (Reference 3 Table 30). The MCNP5 input listing in Reference 3 was setup to run 2400 cycles with 20 skipped cycles; 10,000 histories were used per batch. This specification was used for all runs in this work. The k_{eff} results from this work are presented in Table 2. In this table all uncertainties are at the 68% confidence interval (1 sigma) level. The column heading "UM — 6.1.2" is for the results run with the 6.1.2 version of the code. The column heading "UM — 6.2" is for the results run with the 6.2 version of the code. All average k_{eff} values agree within one standard deviation.

Table 2: Calculated k_{eff} with Standard Deviations

Case	Lattice	CSG	UM – 6.1.2	UM – 6.2
1	1.00478 (17)	1.00502 (17)	1.00536 (17)	1.00536 (17)
2	1.00509 (17)	1.00544 (17)	1.00513 (17)	1.00513 (17)
3	1.00530 (17)	1.00496 (17)	1.00529 (17)	1.00529 (17)
4	1.00550 (17)	1.00533 (17)	1.00540 (17)	1.00540 (17)
5	1.00510 (17)	1.00536 (17)	1.00545 (17)	1.00541 (17)
6	1.00513 (17)	1.00524 (17)	1.00511 (17)	1.00511 (17)
7	1.00529 (17)	1.00539 (17)	1.00531 (17)	1.00531 (17)
8	1.00500 (16)	1.00499 (17)	1.00509 (17)	1.00509 (17)
9	1.00514 (17)	1.00511 (17)	1.00532 (17)	1.00532 (17)
10	1.00541 (17)	1.00539 (17)	1.00522 (17)	1.00522 (17)
Average	1.00517 (21)	1.00522 (19)	1.00527 (13)	1.00526 (12)

The original problem setup was modified to include an F4 volume tally for neutron flux over the individual fuel plates and over all fuel plates. Results are presented in Table 3 where the relative error for all (case) flux values was 0.0002. Average results for the four situations agree within one standard deviation.

Table 3: Total Neutron Flux Over All Fuel Plates

Case	Lattice	CSG	UM — 6.1.2	UM — 6.2
1	2.40137e-3	2.40138e-3	2.40151e-3	2.40151e-3
2	2.40200e-3	2.40171e-3	2.40113e-3	2.40113e-3
3	2.40274e-3	2.40165e-3	2.40116e-3	2.40116e-3
4	2.40179e-3	2.40097e-3	2.40225e-3	2.40225e-3
5	2.40143e-3	2.40180e-3	2.40202e-3	2.40189e-3
6	2.40144e-3	2.40224e-3	2.40170e-3	2.40170e-3
7	2.40114e-3	2.40167e-3	2.40166e-3	2.40166e-3
8	2.40115e-3	2.40147e-3	2.40213e-3	2.40213e-3
9	2.40148e-3	2.40191e-3	2.40226e-3	2.40226e-3
10	2.40192e-3	2.40228e-3	2.40114e-3	2.40175e-3
Average	2.40165e-3	2.40171e-3	2.40170e-3	2.40174e-3
Rel. Err.	0.00020	0.00016	0.00019	0.00017

All calculations for this section were completed on system #1. The calculation times in minutes (computer time minus the problem setup time) are provided in Table 4. Average results are shown with one standard deviation in the time. As expected, tracking with the traditional geometry takes less time than tracking on the UM; in this case by roughly a factor of 3. The new tracking paradigm in version 6.2 is approximately 5% faster than that in the 6.1.2 version.

Table 4: HEU Case 37 Calculation Times (minutes)

Case	Lattice	CSG	UM – 6.1.2	UM – 6.2
1	200.34	189.65	632.76	604.07
2	195.90	188.41	630.70	602.67
3	202.16	187.22	629.30	608.35
4	197.59	191.16	680.17	602.67
5	199.74	194.33	655.79	607.29
6	202.76	197.38	677.52	611.71
7	212.62	205.59	684.68	633.39
8	203.57	191.02	639.26	659.43
9	203.22	190.51	636.70	662.25
10	206.16	208.87	687.38	648.63
Average	202.41 +/- 4.68	194.41 +/- 7.38	655.43 +/- 24.49	624.05 +/- 24.48

5.2 IEU-MET-FAST-007 : Big Ten

Calculations with this problem using the UM were previously done and documented in Reference 4. The current verification work considers the 1st order element cases for both the merged-part and multi-part configurations of the Reference 4 work. All calculations for this work were completed on system #2.

While the Reference 4 work completed one calculation for each case, this work took a slightly different approach. Eighteen independent calculations were completed for each case, including the traditional CSG one, and the results were averaged. For the Reference 4 work, each run used 20,000 histories per cycle with 10 inactive cycles and 150 active cycles. During this work it was discovered that 10 inactive cycles were not sufficient to achieve a converged source, based on Shannon entropy considerations, for all independent runs. Therefore, in the current work 20,000 histories per cycle were used with 30 inactive cycles and 220 active cycles.

Results for this work appear in Tables 5 to 8 where the one standard deviation uncertainties, in parentheses, are expressed for the last two decimal places. While the k_{eff}'s of Tables 5 to 8 are slightly improved over those presented in Table I of Reference 4, the general conclusions have not changed. However, it cannot be stressed enough: users should be wary of coarse mesh models for criticality calculations.

Table 5: Comparison of Big Ten CSG and UM Results – Multi-Part with 1st Order Hex

Number of Elements	Fuel Volume % Error	Refl. Volume % Error	k_{eff}	k_{eff} % error	Runtime (min)
36912	-0.02329	-0.22486	0.995060 (066)	0.010654	64.67
4848	-0.20965	-0.27785	0.994780 (088)	-0.017488	44.02
1944	-0.83704	-0.45590	0.993680 (074)	-0.128046	38.84
984	-9.96840	-2.33053	0.976259 (068)	-1.878981	35.17
CSG	–	–	0.994954 (067)	–	13.20

Table 6: Comparison of Big Ten CSG and UM Results – Multi-Part with 1st Order Tet

Number of Elements	Fuel Volume % Error	Refl. Volume % Error	k_{eff}	k_{eff} % error	Runtime (min)
329718	-0.02329	-0.17904	0.995006 (071)	0.005226	88.27
42395	-0.20965	-0.23699	0.994651 (065)	-0.030454	53.56
12038	-0.83704	-0.40984	0.993722 (050)	-0.123825	45.63
3501	-9.96840	-2.28447	0.976266 (060)	-1.878278	38.61
CSG	–	–	0.994954 (067)	–	13.20

Table 7: Comparison of Big Ten CSG and UM Results – Merged-Part with 1st Order Hex

Number of Elements	Fuel Volume % Error	Refl. Volume % Error	k_{eff}	k_{eff} % error	Runtime (min)
47520	-0.03184	-0.03170	0.995050 (084)	0.009649	58.40
5840	-0.18247	-0.18251	0.994798 (079)	-0.015679	38.82
1920	-0.64137	-0.64114	0.994092 (068)	-0.086637	34.95
480	-2.54995	-2.55043	0.991521 (056)	-0.345041	32.45
CSG	–	–	0.994954 (067)	–	13.20

Table 8: Comparison of Big Ten CSG and UM Results – Merged-Part with 1st Order Tet

Number of Elements	Fuel Volume % Error	Refl. Volume % Error	k_{eff}	k_{eff} % error	Runtime (min)
139526	-0.03339	-0.03343	0.994972 (081)	0.001809	119.38
24233	-0.15995	-0.16047	0.994767 (084)	-0.018795	48.95
10492	-0.64137	-0.64114	0.994010 (064)	-0.094879	39.81
4993	-2.54995	-2.55043	0.991382 (062)	-0.359012	35.71
CSG	–	–	0.994954 (067)	–	13.20

5.3 HEU-MET-FAST-001 : Simple Bare Sphere

Each of the problems discussed in Section 4.3 were run on system #3 with six independent runs and then the results were averaged. For each calculation, 5000 histories were specified per cycle with 100 skip cycles and 1900 active cycles for a total of 2000 cycles.

In the tables that follow, the first column contains the case identifier which is nothing more than the finite element seed value used in generating the UM. Column two is the total number of elements in each case as a result of using the column one seed value in the mesh generation.

With the k_{eff} results of Table 9 are the one standard deviation uncertainties, in parentheses, expressed for the last two decimal places. For example, 0.98041 (11) is 0.98041±0.00011. Of the 12 cases, the UM and CSG results agree within one standard deviation for 5 cases, within two standard deviations for 5 cases, and the remaining 2 cases are at about the three standard deviation level of agreement.

For the total neutron flux results (an F4 tally over the fuel region) of Table 10, almost all errors were determined to be 0.0001 (relative). Except for case 4 where the UM and CSG calculations disagree by 1.3%, the next worse case (0.95) shows a difference of 0.0338%. Overall agreement is fairly consistent with the k_{eff} results.

Table 9: Godiva k_{eff} Comparison

Case / Seed	Number of Cells / Elements	UM	CSG	UM/CSG
4	1375	0.98041 (11)	0.98032 (06)	1.000089
3	3142	0.98908 (06)	0.98902 (09)	1.000056
2	9722	0.99638 (08)	0.99617 (09)	1.000216
1.7	13305	0.99684 (04)	0.99689 (12)	0.999950
1.5	16349	0.99750 (06)	0.99727 (07)	1.000228
1.1	39250	0.99926 (13)	0.99904 (07)	1.000215
1	51336	0.99964 (14)	0.99940 (07)	1.000235
0.95	59160	0.99986 (10)	0.99948 (09)	1.000376
0.80	93593	1.0002 (11)	1.0002 (14)	1.000055
0.65	161971	1.0005 (09)	1.0005 (05)	1.000067
0.50	320069	1.0010 (08)	1.0007 (13)	1.000228
0.45	401723	1.0010 (07)	1.0009 (07)	1.000113

Table 10: Comparison of Godiva Fuel Volume Tallies

Case / Seed	Number of Cells / Elements	UM	CSG	UM/CSG
4	1375	2.5547e-03	2.5878e-03	0.987209
3	3142	2.4963e-03	2.4963e-03	1.000020
2	9722	2.4523e-03	2.4519e-03	1.000167
1.7	13305	2.4473e-03	2.4474e-03	0.999963
1.5	16349	2.4437e-03	2.4433e-03	1.000160
1.1	39250	2.4328e-03	2.4324e-03	1.000173
1	51336	2.4309e-03	2.4303e-03	1.000226
0.95	59160	2.4298e-03	2.4289e-03	1.000338
0.80	93593	2.4265e-03	2.4264e-03	1.000033
0.65	161971	2.4245e-03	2.4245e-03	1.000033
0.50	320069	2.4227e-03	2.4223e-03	1.000198
0.45	401723	2.4223e-03	2.4220e-03	1.000120

5.4 Kobayashi Analytical Benchmark

A total of 16 problems were run with Kobayashi problem #1, as described above in Section 4.4 using system #2 with the MPI version of the code (1 master process and 143 slave processors with 1 OpenMP task per processor). There were 4 UM arrangements: Attila (1st order tets) – coarse and fine mesh and Abaqus 1st order tets and 1st order hexs. Each of these had pure absorber material assignments and 50/50 material assignments. Each mesh / material arrangement was run with MG and CE cross sections. The pure absorber cases were run with 1 million histories. The 50/50 material cases were run with 100 million histories. Note that FSD is fractional standard deviation, i.e., relative error.

Each calculation had 30 point detectors (F5 tallies) along 3 traverses in the geometry that are grouped and identified as cases 1A, 1B, and 1C. This is consistent with the Reference 7 work. Case 1A traverses every 10 cm in y from 5 to 95 cm, inclusive, keeping $x = z = 5$ cm. Case 1B traverses along the diagonal with $x = y = z = 5$, 15, 25, ..., 95 cm. Case 1C traverses every 10 cm in x from 5 to 95 cm, inclusive, with $y = 55$ cm and $z = 5$ cm. This set of detectors resulted in one duplication of position in the source volume: $x = 5$, $y = 5$, $z = 5$ (seen as the first point in Cases 1A and 1B).

The exclusion sphere for the Case 1A point detector at $x = 5$, $y = 5$, $z = 5$ was set to 1 cm because source particles that were generated in the vicinity of the detector would lead to wild variances and bad statistics in the tally for that detector [13]. To see that effect, the exclusion radius for the Case 1B point detector at $x = 5$, $y = 5$, $z = 5$ was set to 0.01 cm. Exclusion spheres for all of the remaining detectors were also set at 0.01 cm. This is in contrast to the Reference 13 work that set the exclusion sphere to 5 cm for the 50/50 material calculations.

As with the Reference 12 work, the only variance reduction used in this work was the implicit capture and weight cutoff games. Consequently, some results from this work do not compare as favorably as those from Reference 13, but are consistent with the Reference 12 work. Ultimately, all of the results from the current work agree well enough to conclude that the feature is working correctly. It should be noted that agreement between these calculations and the benchmark values can be improved to the levels demonstrated in Reference 13 by reintroducing variance

reduction techniques such as non-uniform cell-based importances or weight windows defined on a cell-wise or mesh-wise basis. This will probably be done in the future when V&V suites are established for the UM.

Because of space concerns in this document, Tables 11 to 14 provide a select subset of the results. Table 11 provides the point detector results from the 100% absorber case using the Abaqus 1st order hex mesh model with the CE cross sections. A comparison of the two value at the 5, 5, 5 location show the effect of the two different exclusion radii in the source region. The worst comparison in this table is for the 5, 5, 5 location with the small (0.1 cm) exclusion radius.

Table 12 provides representative results for the 50% absorber / 50% scattering case. This calculation used the Attila4MC coarse mesh model with the MG cross sections. This set of results was selected because included here is the worse comparison of any of the MCNP6 results to the GMVP results of Reference 7 — Case 1B, location 95, 95, 95. The agreement is just outside the 2-sigma confidence level, but the relative error on the MCNP6 result is well above the recommendation of tally reliability and did not pass the 10 statistical checks [21].

Table 13 compares all of the MCNP6 results for the point detector at location 95, 95, 95 with the corresponding GMVP result [7]. Closer agreement exists for all of the calculations not presented in Table 12 for this location. The agreement in Table 13 can be contrasted with that in Table 14 that provides a similar comparison for location 55, 55, 55. What this clearly shows is a need for better variance reduction to more adequately sample the phase space in the vicinity of the point detectors that are a longer way from the source region.

Table 11: Kobayashi Results for the 100% Absorber Case Using the Abaqus 1st Order Hex Mesh with CE Cross sections.

Case	Location (cm)	Analytic Total Flux	MCNP6 Total Flux	FSD (%)	Difference (%)
1A	5,5,5	5.95659e+00	5.9179e+00	0.751	-0.650
	5,15,5	1.37185e+00	1.3720e+00	0.163	0.011
	5,25,5	5.00871e-01	5.0086e-01	0.102	-0.002
	5,35,5	2.52429e-01	2.5246e-01	0.087	0.012
	5,45,5	1.50260e-01	1.5029e-01	0080	0.020
	5,55,5	5.95286e-02	5.9544e-02	0.076	0.026
	5,65,5	1.53283e-02	1.5332e-02	0.072	0.024
	5,75,5	4.17689e-03	4.1780e-03	0.070	0.027
	5,85,5	1.18533e-03	1.1857e-03	0.068	0.031
	5,95,5	3.46846e-04	3.4694e-04	0.067	0.027
1B	5,5,5	5.95659e+00	5.7581e+00	0.937	-3.332
	15,15,15	4.70754e-01	4.7014e-01	0.124	-0.130
	25,25,25	1.69968e-01	1.6987e-01	0.080	-0.058
	35,35,35	8.68334e-02	8.6798e-02	0.070	-0.041
	45,45,45	5.25132e-02	5.2496e-02	0.065	-0.033
	55,55,55	1.33378e-02	1.3334e-02	0.062	-0.028
	65,65,65	1.45867e-03	1.4582e-03	0.060	-0.032
	75,75,75	1.75364e-04	1.7531e-04	0.060	-0.031
	85,85,85	2.24607e-05	2.2453e-05	0.059	-0.034
	95,95,95	3.01032e-06	3.0093e-06	0.059	-0.034
1C	5,55,5	5.95286e-02	5.9544e-02	0.076	0.026
	15,55,5	5.50247e-02	5.5029e-02	0.074	0.008
	25,55,5	4.80754e-02	4.8077e-02	0.072	0.003
	35,55,5	3.96765e-02	3.9678e-02	0.070	0.004
	45,55,5	3.16366e-02	3.1637e-02	0.069	0.001
	55,55,5	2.35303e-02	2.3531e-02	0.068	0.003
	65,55,5	5.83721e-03	5.8372e-03	0.068	0.000
	75,55,5	1.56731e-03	1.5672e-03	0.068	-0.007
	85,55,5	4.53113e-04	4.5307e-04	0.067	-0.009
	95,55,5	1.37079e-04	1.3706e-04	0.066	-0.014

Table 12: Kobayashi Results for the 50/50 Case Using the Attila4MC Coarse 1st Order Tet Mesh with MG Cross sections.

Case	Location (cm)	GMVP Total Flux	FSD (%)	MCNP6 Total Flux	FSD (%)	Difference (%)
1A	5,5,5	8.29260e+00	0.021	8.2969e+00	0.064	0.052
	5,15,5	1.87028e+00	0.005	1.8703e+00	0.015	0.001
	5,25,5	7.13986e-01	0.003	7.1401e-01	0.010	0.003
	5,35,5	3.84685e-01	0.004	3.8467e-01	0.009	-0.004
	5,45,5	2.53984e-01	0.006	2.5404e-01	0.018	0.022
	5,55,5	1.37220e-01	0.073	1.3696e-01	0.356	-0.189
	5,65,5	4.65913e-02	0.117	4.6199e-02	0.409	-0.842
	5,75,5	1.58766e-02	0.197	1.5738e-02	0.667	-0.873
	5,85,5	5.47036e-03	0.343	5.3430e-03	0.852	-2.328
	5,95,5	1.85082e-03	0.619	1.8264e-03	2.012	-1.319
1B	5,5,5	8.29260e+00	0.021	8.2750e+00	0.226	-0.212
	15,15,15	6.63233e-01	0.004	6.6325e-01	0.011	0.003
	25,25,25	2.68828e-01	0.003	2.6881e-01	0.008	-0.007
	35,35,35	1.56683e-01	0.005	1.5669e-01	0.012	0.004
	45,45,45	1.04405e-01	0.011	1.0443e-01	0.028	0.024
	55,55,55	3.02145e-02	0.061	3.0429e-02	0.762	0.710
	65,65,65	4.06555e-03	0.074	4.0730e-03	1.262	0.183
	75,75,75	5.86124e-04	0.116	5.7848e-04	2.103	-1.304
	85,85,85	8.66059e-05	0.198	8.6898e-05	4.967	0.0337
	95,95,95	1.12892e-05	0.383	1.7009e-05	24.270	50.666
1C	5,55,5	1.37220e-01	0.073	1.3696e-01	0.356	-0.189
	15,55,5	1.27890e-01	0.076	1.2712e-01	0.352	-0.602
	25,55,5	1.13582e-01	0.080	1.1262e-01	0.424	-0.847
	35,55,5	9.59578e-02	0.088	9.7148e-02	1.544	1.240
	45,55,5	7.82701e-02	0.094	7.8824e-02	1.024	0.708
	55,55,5	5.67030e-02	0.111	5.6485e-02	0.551	-0.384
	65,55,5	1.88631e-02	0.189	1.8613e-02	0.547	-1.326
	75,55,5	6.46624e-03	0.314	6.3458e-03	0.862	-1.863
	85,55,5	2.28099e-03	0.529	2.2388e-03	1.148	-1.850
	95,55,5	7.93924e-04	0.890	7.6530e-04	1.616	-3.605

Table 13: Comparison of MCNP6 Total Flux at Case 1B Location 95, 95, 95

Calculation	Total Flux	FSD (%)	Difference (%)
GMVP	1.12892e-05	0.383	—
Attila4MC Coarse Mesh - MG	1.7009e-05	24.270	50.666
Attila4MC Coarse Mesh - CE	1.0650e-05	8.507	-5.662
Attila4MC Fine Mesh - MG	1.0953e-05	7.083	-2.978
Attila4MC Fine Mesh - CE	1.2043e-05	7.916	6.677
Abaqus 1st Hexs – MG	9.3545e-06	3.697	-17.137
Abaqus 1st Hexs – CE	9.8012e-06	4.112	-13.181
Abaqus 1st Tets – MG	9.4208e-06	3.173	-16.550
Abaqus 1st Tets – CE	1.0054e-05	5.264	-10.941

Table 14: Comparison of MCNP6 Total Flux at Case 1B Location 55, 55, 55

Calculation	Total Flux	FSD (%)	Difference (%)
GMVP	3.02145e-02	0.061	—
Attila4MC Coarse Mesh - MG	3.0429e-02	0.762	0.710
Attila4MC Coarse Mesh - CE	3.1037e-02	1.107	2.722
Attila4MC Fine Mesh - MG	3.0002e-02	0.815	-0.7033
Attila4MC Fine Mesh - CE	2.9880e-02	0.546	-1.107
Abaqus 1st Hexs – MG	2.9787e-02	0.433	-1.415
Abaqus 1st Hexs – CE	2.9822e-02	0.487	-1.299
Abaqus 1st Tets – MG	3.0045e-02	0.502	-0.561
Abaqus 1st Tets – CE	3.0107e-02	0.464	-0.356

5.5 Ueki Neutron Shielding Benchmark

In the Reference 15 work, the ^{252}Cf point source was positioned at $x = 0.001$ cm. Initial calculations for this work with the KRAFTON material were completed with the source point at this location. A comparison of UM results to CSG results always showed the UM results lower than the CSG ones. With the 35 cm thick shield the UM was lower by ~3%. In terms of confidence intervals (C.I.), agreement would exist only at the 10 to 11 C.I. level. The reason for this is associated with the differences in the geometries and is explained next.

The Abaqus 1st order hex model from Reference 15 was re-meshed with a smaller seed on the edges of the conical cutout in order to produce a higher-fidelity UM model in this region. The apex of the conical cutout is shown in Figure 4 where four 1st order hexahedra meet. The black line that extents from the apex, through the upper left (paraffin) hex, and out to the left is the track of a particle that in the CSG model does not intersect the paraffin block! What Figure 4 shows is that the meshing at the apex of the cone, despite the initial refinement, produces an inadequate representation of the geometry in this region. Consequently, a small fraction of source particles are interacting with the paraffin in the UM geometry where they are not doing this in the CSG. These particles are knocked down in energy sooner than with the CSG model thus contributing less to the tallies — hence an under prediction of the results. When the source location is moved out further along the x-axis, results between CSG and UM come into agreement. A series of calculations were performed to demonstrate this. As a result,

a source location of $x = 0.5$ cm was chosen for the (CSG and both UM) calculations in this work.

Neither Reference 14 or 16 provide any details about the spatial extents of the ^{252}Cf source. It is inconceivable that the source was suspended in mid-air without being inside some small container. The figures in both references indicate a point source at the $x = 0$ cm location. The figures also clearly show that the apex of the cone does not begin at the $x = 0$ cm location, but at some small distance further along the negative x-axis. While assuming that the apex of the conical cutout begins at $x = 0$ cm may be acceptable for the CSG models, it is probably not correct. For the UM models, the mesh needs to be refined (more and smaller) near the apex location; this can be done. However, what is needed are details on the actual location of the apex and whether it is truly a point or has some type of radius.

It is noted that moving the source slightly along the positive x-axis improved the agreement between the calculational results and experiment results from Table 2 of Reference 14. However, this was not enough to achieve acceptable agreement for all shield thicknesses.

Figure 4: Unstructured mesh model of paraffin cone apex in Ueki model.

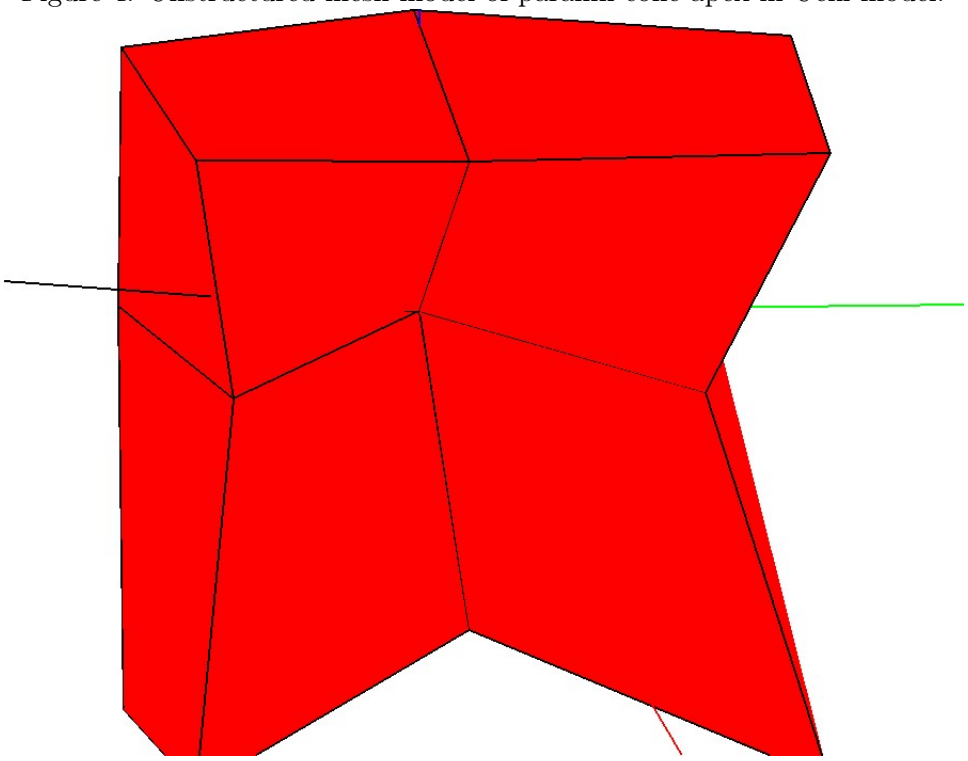

In Tables 15 to 20 the calculational results for the KRAFTON shield are compared with the experimental results from Table 2 of Reference 14. All calculations were performed on system #2. (Note that there were no experimental results for a 2 cm thick shield.) The general take away is that the calculations, irrespective of the MCNP6 geometry model, under predict the experimental results, even when the shield doesn't exist or the shield is thin. This is particularly troubling for the no shield cases. This indicates a problem with not modeling the experiment as it was done. Several factors may be contributing to this and lead to a couple of questions: 1) Is modeling of the physical detector important? 2) Was there anything else in the room of

significance (support for the experimental equipment such as a table) that should be modeled?

Reference 14 provides a brief discussion of the neutron dosimeter, but not enough details from which to construct a model. Likewise, Reference 16 mentions an ALOKA survey meter, but provides no details. Neither reference provides details of other equipment in the room at the time of the experiment.

Relative to experiment, the MCNP6 results — irrespective of model — under predict experiment by ~22% with the 35 cm shield. The MCNP6 results are consistent and agree within 1 standard deviation. The maximum disagreement from the CSG models was ~3.6% for the F4 tally in the unshielded Attila2MC model; the disagreement for the F5 tally for this model was ~1.1%. Otherwise, for all other cases, the maximum difference was 0.7% for the F4 tallies and 0.2% for the F5 tallies. All calculations were done with 10 million histories.

Table 15: Ueki benchmark with KRAFTON material — F4 tally results / CSG

Thickness (cm)	Experiment	F4	Rel. Error	C/M	Exp. Atten.	Calc. Atten.
0	524.6	481.50	0.0382	0.9178	1.0000	1.0000
2	–	407.83	0.0247	–	–	0.8470
5	290.9	291.77	0.0152	1.0030	0.5545	0.6060
10	151.7	150.58	0.0095	0.9926	0.2892	0.3127
15	81.1	75.05	0.0085	0.9254	0.1546	0.1559
20	41.6	37.98	0.0078	0.9131	0.0793	0.0789
25	22.2	19.44	0.0076	0.8755	0.0423	0.0404
30	12	9.96	0.0076	0.8296	0.0229	0.0207
35	6.6	5.26	0.0078	0.7976	0.0126	0.0109

Table 16: Ueki benchmark with KRAFTON material — F5 tally results / CSG

Thickness (cm)	Experiment	F5	Rel. Error	C/M	Exp. Atten.	Calc. Atten.
0	524.6	514.80	0.0016	0.9813	1.0000	1.0000
2	–	418.30	0.0016	–	–	0.8125
5	290.9	292.04	0.0020	1.0039	0.5545	0.5673
10	151.7	150.39	0.0020	0.9914	0.2892	0.2921
15	81.1	75.59	0.0022	0.9320	0.1546	0.1468
20	41.6	38.26	0.0023	0.9197	0.0793	0.0743
25	22.2	19.44	0.0025	0.8757	0.0423	0.0378
30	12	10.03	0.0028	0.8354	0.0229	0.0195
35	6.6	5.23	0.0031	0.7918	0.0126	0.0102

Table 17: Ueki benchmark with KRAFTON material – F4 tally results / Attila4MC UM

Thickness	Experiment	F4	Rel. Error	C/M	Exp. Atten.	Calc. Atten.
0	524.6	498.89	0.0522	0.9510	1.0000	1.0000
2	–	410.93	0.0240	–	–	0.8605
5	290.9	289.33	0.0151	0.9946	0.5545	0.5799
10	151.7	149.93	0.0094	0.9883	0.2892	0.3005
15	81.1	75.57	0.0083	0.9318	0.1546	0.1515
20	41.6	38.04	0.0077	0.9144	0.0793	0.0762
25	22.2	19.46	0.0077	0.8768	0.0423	0.0390
30	12	9.94	0.0077	0.8280	0.0229	0.0199
35	6.6	5.19	0.0078	0.7864	0.0126	0.0104

Table 18: Ueki benchmark with KRAFTON material – F5 tally results / Attila4MC UM

Thickness (cm)	Experiment	F5	Rel. Error	C/M	Exp. Atten.	Calc. Atten.
0	524.6	520.68	0.0130	0.9925	1.0000	1.0000
2	–	418.10	0.0016	–	–	0.8123
5	290.9	291.75	0.0020	1.0029	0.5545	0.5603
10	151.7	150.56	0.0020	0.9925	0.2892	0.2892
15	81.1	75.72	0.0022	0.9337	0.1546	0.1454
20	41.6	38.31	0.0023	0.9208	0.0793	0.0736
25	22.2	19.47	0.0025	0.8768	0.0423	0.0374
30	12	10.04	0.0028	0.8367	0.0229	0.0193
35	6.6	5.22	0.0031	0.8916	0.0126	0.0100

Table 19: Ueki benchmark with KRAFTON material – F4 tally results / Abaqus UM

Thickness (cm)	Experiment	F4	Rel. Error	C/M	Exp. Atten.	Calc. Atten.
0	524.6	477.53	0.0371	0.9103	1.0000	1.0000
2	–	407.16	0.0252	–	–	0.8526
5	290.9	287.89	0.0151	0.9867	0.5545	0.6029
10	151.7	148.23	0.0092	0.9771	0.2892	0.3104
15	81.1	75.15	0.0084	0.9267	0.1546	0.1574
20	41.6	38.15	0.0076	0.9170	0.0793	0.0799
25	22.2	19.35	0.0077	0.8715	0.0423	0.0405
30	12	10.02	0.0076	0.8350	0.0229	0.0210
35	6.6	5.20	0.0077	0.7882	0.0126	0.0109

Table 20: Ueki benchmark with KRAFTON material – F5 tally results / Abaqus UM

Thickness (cm)	Experiment	F5	Rel. Error	C/M	Exp. Atten.	Calc. Atten.
0	524.6	514.73	0.0011	0.9812	1.0000	1.0000
2	–	418.75	0.0016	–	–	0.8135
5	290.9	292.13	0.0019	1.0042	0.5545	0.5675
10	151.7	150.19	0.0020	0.9900	0.2892	0.2918
15	81.1	75.74	0.0022	0.9339	0.1546	0.1471
20	41.6	38.24	0.0023	0.9191	0.0793	0.0743
25	22.2	19.45	0.0025	0.8762	0.0423	0.0378
30	12	10.03	0.0028	0.8357	0.0229	0.0195
35	6.6	5.23	0.0031	0.7923	0.0126	0.0102

In Tables 21 to 23 the calculational results for the graphite shield are compared with the experimental attenuation results where the lin-log plot provided in Reference 16 Figure 7-2 was digitized [17] to extract the experimental dose attenuation factors for graphite. Unlike the KRAFTON results discussed above, the MCNP6 results under predict the attenuation. The F4 tallies produce the maximum deviation of ~17% while the F5 tallies produce a maximum deviation of ~8%.

The MCNP6 results are consistent and agree within 1 standard deviation. The maximum disagreement from the CSG models was ~3.6% for the F4 tally in the unshielded Attila model; the disagreement for the F5 tally for this model was ~1.1%. Otherwise, for all other cases, the maximum difference was 0.5% for the F4 tallies and 0.4% for the F5 tallies. All calculations were done with 10 million histories.

Table 21: Ueki benchmark with graphite shield — F4 / F5 tally results / CSG

Thickness (cm)	F4	Rel. Error	F5	Rel. Error	Exp. Atten.	F4 Atten.	F5 Atten.
0	481.50	0.0382	514.80	0.0016	1.0000	1.0000	1.0000
2	424.28	0.0281	450.69	0.0018	0.8634	0.8812	0.8755
5	374.86	0.0191	380.45	0.0024	0.7046	0.7785	0.7390
10	280.31	0.0117	280.01	0.0027	0.5028	0.5822	0.5439
15	198.22	0.0085	198.95	0.0029	0.3580	0.4117	0.3865
20	137.46	0.0067	137.84	0.0029	0.2479	0.2885	0.2678
25	82.42	0.0062	92.79	0.0032	0.1673	0.1919	0.1802
30	62.13	0.0058	62.10	0.0032	0.1117	0.1290	0.1206
35	41.14	0.0059	41.12	0.0036	0.0745	0.0854	0.0799

Table 22: Ueki benchmark with graphite shield — F4 / F5 tally results / Attila

Thickness (cm)	F4	Rel. Error	F5	Rel. Error	Exp. Atten.	F4 Atten.	F5 Atten.
0	498.89	0.0522	520.68	0.0130	1.0000	1.0000	1.0000
2	429.46	0.0283	449.73	0.0013	0.8634	0.8608	0.8637
5	376.54	0.0190	379.94	0.0024	0.7046	0.7548	0.7297
10	279.79	0.0118	279.83	0.0027	0.5028	0.5608	0.5374
15	199.23	0.0086	198.56	0.0029	0.3580	0.3993	0.3813
20	136.91	0.0067	137.71	0.0030	0.2479	0.2744	0.2645
25	92.59	0.0070	92.97	0.0048	0.1673	0.1856	0.1786
30	62.27	0.0059	62.09	0.0031	0.1117	0.1248	0.1193
35	41.15	0.0063	41.17	0.0039	0.0745	0.0825	0.0791

Table 23: Ueki benchmark with graphite shield – F4 / F5 tally results / Abaqus

Thickness (cm)	F4	Rel. Error	F5	Rel. Error	Exp. Atten.	F4 Atten.	F5 Atten.
0	477.53	0.0371	514.73	0.0011	1.0000	1.0000	1.0000
2	422.95	0.0282	450.14	0.0013	0.8634	0.8478	0.8645
5	371.51	0.0193	380.10	0.0023	0.7046	0.7780	0.7384
10	279.86	0.0116	280.50	0.0025	0.5028	0.5861	0.5449
15	199.04	0.0084	199.56	0.0030	0.3580	0.4168	0.3879
20	138.02	0.0073	138.41	0.0041	0.2479	0.2890	0.2689
25	92.87	0.0064	92.91	0.0035	0.1673	0.1945	0.1805
30	62.41	0.0067	62.14	0.0046	0.1117	0.1307	0.1207
35	41.16	0.0064	41.04	0.0040	0.0745	0.0862	0.0797

Figures 5 and 6 plot the experimental dose attenuation factors with assumed 5% error bars. The F4 and F5 tally results from the CSG runs are co-plotted in these figures and are well within the error bars. UM F4 and F5 tally results are not plotted because there is little deviation between them and the CSG results.

Figure 5: Ueki neutron attenuation results for KRAFTON N2.

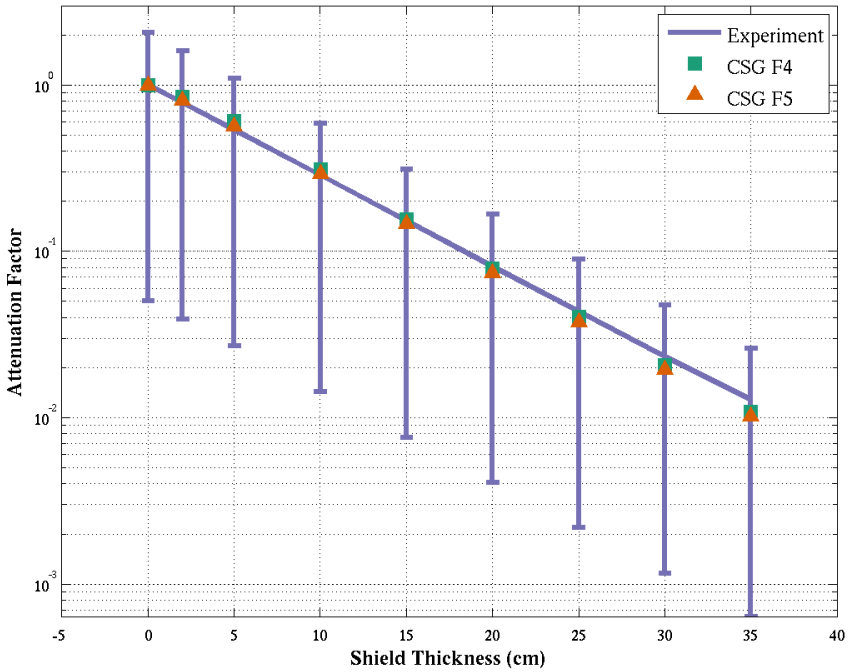

Figure 6: Ueki neutron attenuation results for graphite.

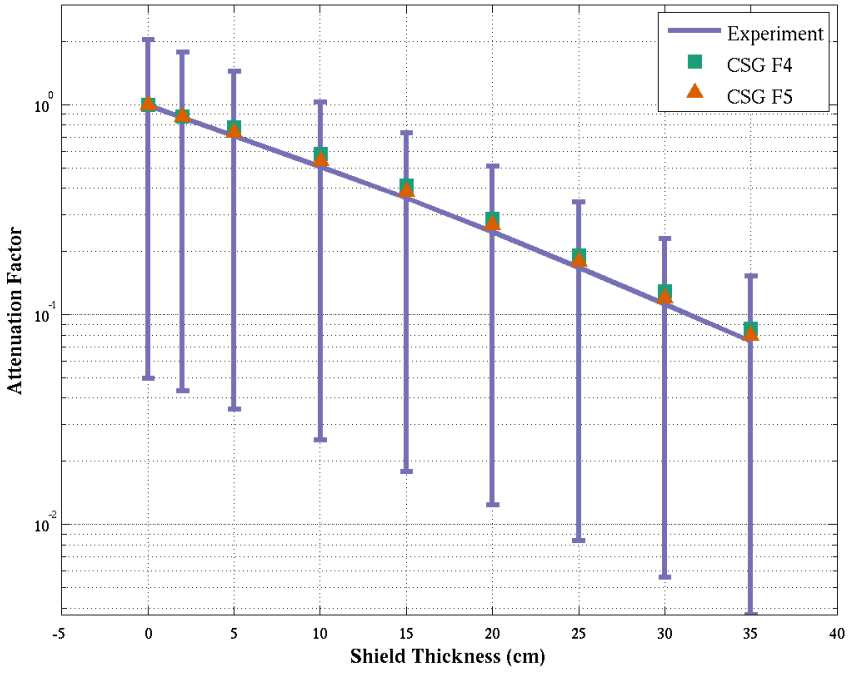

While all MCNP6 calculations show significant disagreement from the experimental results, the CSG and UM results agree well (within 1 standard deviation) with each other and again provide evidence that the UM tracking routines yield acceptable results.

6 Summary

For MCNP Version 6.2, the UM top-level tracking routine (`regl_track_um`) has been refactored to make the code less convoluted and to make it faster, at least in some cases. Consequently, the code must be verified and validated to ensure that is is functioning as intended and producing acceptable results. To that end, this report documents a number of test problems that were analyzed. A future report will discuss performance.

The `regl_track_um` routine is used by all currently supported particle types [2] in the code as well as the point detector and DXTRAN features. Test problems in this report tracked neutrons and photons. Point detector tallies were used in some problems. Calculations were performed on a variety of computer systems with OpenMP only and OpenMPI/OpenMP versions of the code. Test problems covered criticality and fixed sources. Comparisons were also made to analytical benchmarks. Results from UM calculations were also compared to equivalent CSG calculations. Comparisons in this report demonstrate that the UM with the refactored top-level tracking routine is producing acceptable results in agreement with those calculated from equivalent CSG models. Deviation of calculated to measured quantities for the problems considered here are consistent for both UM and CSG models.

References

[1] D. B. Pelowitz, A. J. Fallgren, and G. E. McMath, "MCNP6 User's Manual: Code Version 6.1.1 beta," Tech. Rep. LA-CP-14-00745, Los Alamos National Laboratory, Los Alamos, NM, USA, June 2014.

[2] R. L. Martz, "The MCNP6 Book On Unstructured Mesh Geometry: User's Guide for MCNP 6.2," Tech. Rep. LA-UR-17-22442, Los Alamos National Laboratory, Los Alamos National Laboratory, March 2017.

[3] "International Handbook of Evaluated Criticality Safety Benchmark Experiments," Tech. Rep. NEA/NSC/DOC(95)03/I-IX, Organization for Economic Co-operation and Development — Nuclear Energy Agency (OECD-NEA), Paris, France, September 2013.

[4] T. P. Burke *et al.*, "Reactor Physics Verification of the MCNP6 Unstructured Mesh Capability," in *International Conference on Mathematics and Computational Methods Applied to Nuclear Science & Engineering (M&C 2013)*, (Sun Valley, ID, USA, May 5–9, 2013), American Nuclear Society, 2013.

[5] R. L. Martz and K. M. Marshall, "A Notable Comparison of Computational Geometries in MCNP6 Calculations," *Nuclear Technology*, vol. 184, pp. 239–248, November 2013.

[6] D. J. Whalen *et al.*, "MCNP: Neutron Benchmark Problems," Tech. Rep. LA-12212, Los Alamos National Laboratory, Los Alamos, NM, USA, November 1991.

[7] K. Kobayashi, N. Sugimura, and Y. Nagaya, "3-D Radiation Transport Benchmark Problems and Results for Simple Geometries with Void Regions," Tech. Rep. NEA/NSC/DOC(2000), Organization for Economic Co-operation and Development / Nuclear Energy Agency, Paris, France, 2000.

[8] T. Mori and M. Nakagawa, "MVP/GMVP: General Purpose Monte Carlo Codes for Neutron and Photon Transport Calculations Based on Continuous Energy and Multi-group Methods," Tech. Rep. JAERI-DATA / Code 94-007, Japan Atomic Energy Research Institute, 1994.

[9] Dassault Systèmes Simulia Corporation, "Abaqus/CAE 6.14 Online Documentation," 2014.

[10] Varax Imaging Systems, "Attila with MCNP Integration: Attila4MC." http://www.vareximaging.com/products/attila-software. Current as of February 8, 2017.

[11] J. A. Kulesza and R. L. Martz, "MCNP6 Unstructured Mesh Tutorial Using Abaqus/CAE 6.12-1," Tech. Rep. LA-UR-15-25143, Los Alamos National Laboratory, Los Alamos, NM, USA, July 2015.

[12] J. A. Kulesza and R. L. Martz, "Evaluation of the Kobayashi Analytical Benchmark Using MCNP6's Unstructured Mesh Capabilities," *Nuclear Technology*, vol. 195, pp. 55–70, July 2016.

[13] B. E. Toth and F. B. Brown, "MCNP5 Benchmark Calculations for 3-D Radiation Transport in Simple Geometries with Void Regions," Tech. Rep. LA-UR-03-5974, Los Alamos National Laboratory, Los Alamos, NM, USA, 2003.

[14] K. Ueki, A. Ohashi, and Y. Anayama, "Neutron Shielding Ability of KRAFTON N2-Mannan-KRAFTON N2 Sandwich-Type Material and Others," in *Proceedings of Radiation Protection and Shielding Division Topical Meeting*, (Pasco, WA, USA April 26–May 1, 1992), pp. 130–137, American Nuclear Society, 1992.

[15] J. A. Kulesza and R. L. Martz, "Evaluation of Pulsed Sphere Time-of-Flight and Neutron Attenuation Experimental Benchmarks Using MCNP6's Unstructured Mesh Capabilities," *Nuclear Technology*, vol. 195, pp. 44–54, July 2016.

[16] K. Ueki, A. Ohashi, N. Nariyama, S. Nagayama, T. Fujita, K. Hattori, and Y. Anayama, "Systematic Evaluation of Neutron Shielding Effects for Materials," *Nuclear Science and Engineering*, vol. 124, pp. 455–464, November 1996.

[17] M. Mitchell *et al.*, "Engauge Digitizer Software, Version 9.7." http://markummitchell.github.io/engauge-digitizer/, March 2017.

[18] S. W. Mosher, S. R. Johnson, A. M. Bevill, A. M. Ibrahim, C. R. Daily, T. M. Evans, J. C. Wagner, J. O. Johnson, and R. E. Grove, "ADVANTG—An Automated Variance Reduction Parameter Generator," Tech. Rep. ORNL/TM-2013/416, Rev. 1, Oak Ridge National Laboratory, Oak Ridge, TN, USA, November 2015.

[19] R. J. McConn Jr., C. J. Gesh, R. T. Pagh, R. A. Rucker, and R. G. Williams III, "Compendium of Material Composition Data for Radiation Transport Modeling," Tech. Rep. PNNL-15870, Rev. 1, Pacific Northwest National Laboratory, Richland, WA, USA, 2011.

[20] "Neutron and Gamma-Ray Flux-to-Dose-Rate Factors," Tech. Rep. ANSI/ANS 6.1.1-1977, American Nuclear Society, La Grange Park, IL, USA, 1977.

[21] XCP-5: Monte Carlo Team, "MCNP — A General N-Particle Transport Code, Version 5, Volume 1: Overview and Theory," Tech. Rep. LA-UR-03-1987, Los Alamos National Laboratory, Los Alamos, NM, USA, 2005.